View Online / Journal Homepage / Table of Contents for this issue

Hydroxyapatite supported antibacterial Ag_3PO_4 nanoparticles†

Joanna J. Buckley,[a] Adam F. Lee,*[b] Luca Olivi[c] and Karen Wilson[b]

Received 18th May 2010, Accepted 20th July 2010
DOI: 10.1039/c0jm01500h

High surface area hydroxyapatites have been explored as biocompatible supports for antibacterial applications. Porosimetry, XRD, XPS and XAS reveal that Ag-doped mesoporous hydroxyapatite promotes the genesis of potent Ag_3PO_4 nanoparticles, effective against *Staphylococcus aureus* and *Pseudomonas aeruginosa*.

Published on 16 August 2010 on http://pubs.rsc.org | doi:10.1039/C0JM01500H
Downloaded by Cardiff University on 02 April 2012

Introduction

Hydroxyapatite ($Ca_{10}(PO_4)_6(OH)_2$ or HA) is a major component of bone, and the combination of biocompatibility and structural rigidity facilitates its use as medical support architectures within the body as surgical implants[1–3] and to aid tissue regeneration. However, an important complication with the use of such biomaterials is their propensity for biofilm formation, initiated through reversible bacterial adhesion at their outer surfaces *via* weak van der Waals forces.[4,5] Biofilm growth can be strongly suppressed by inhibiting this step,[6] whereas once bacteria gain this first foothold they provide an improved environment for further bacteria adhesion, becoming irreversibly bound to each other as well as the host surface as colonies develop, forming a complex, toxic matrix.[7] MRSA and other hospital acquired infections are commonly spread in this manner, and have been treated with transition metals such as Cu, Zn and Ni, known to exhibit antibacterial properties.[8,9] Silver has also long been noted for its bactericidal nature, and it is very effective in killing biofilms.[1] The first documented use of silver in water purification dates back to ancient Greece, where silver coins were added to water vessels to prevent bacterial growth, while the Phoenicians used silver jars to preserve wine and vinegar during long military and exploratory campaigns. The first scientific papers detailing silver's medicinal benefits for the treatment of eye infections were published in the 1880s, wherein dilute silver nitrate solutions helped alleviate blindness in infants.[10] Topical silver treatments were subsequently extended to burns in 1965,[11] with silver sulfadiazine (SSD), a soluble Ag(I) complex, introduced to reduce wound infections in 1968,[12,13] an important treatment that remains in use today. This increased awareness of silver as an antimicrobial agent has led to the synthesis of various inorganic Ag-containing materials including zeolites,[14] resin composites,[15] and glasses.[16] It is generally accepted that silver's biological activity is associated with release of dissolved Ag^+ ions,[17,18] explaining the efficacy of SSD in treating skin wounds.

Silver has been incorporated into many presentation formats with a view to improving/regulating its release rate *in vivo*.[19–24] We recently showed that simple wet-impregnation of ultra-low silver concentrations over mesoporous alumina generated highly dispersed (5 nm) Ag_2CO_3 nanoparticles with excellent antibacterial properties.[25] However, an important issue in developing therapeutic treatments to combat infection is the cyto/biocompatibility of associated dressing or device format.[26,27] While alumina is FDA-approved for various drug and prosthetic applications, it is not widely used in wound dressings. In contrast, HA has been widely employed to present colloidal silver nanoparticles (7–65 nm)[28–30] or form ion-exchanged, Ag-doped HA coatings and scaffolds with antimicrobial properties.[30–34] Here we apply X-ray probes to show that high area HAs offer biocompatible, solid supports able to preferentially stabilise Ag_3PO_4 nanoparticles affording tuneable Ag(I) release rates and potent bactericidal activity.

Materials and methods

Hydroxyapatite and calcium phosphate synthesis

High area hydroxyapatite (HA-H) was prepared following the synthesis of El Hammari *et al.*[35] Briefly, 14.96 g $Ca(OH)_2$ was dissolved in 200 cm^3 H_2O/EtOH (1 : 1 vol%), and stirred for 3 h at 25 °C. Subsequently, 13.40 g $NH_4H_2PO_4$ were dissolved in 200 cm^3 water and slowly added to the $Ca(OH)_2$ solution over 24 h *via* dropwise addition. The pH of the slurry was monitored throughout the precipitation reaction and reached a final value of around 11. The slurry was then heated at 70 °C under reflux and stirring for 3 h. The resulting precipitated crystals were aged for 24 h, filtered and then calcined overnight at 100 °C to give a final bright white powder product.

Comparative low area hydroxyapatite (HA-L) was prepared by Plasma Biotal Ltd.[2] by calcining 100 g of amorphous calcium phosphate (CAPTAL® A.C.P) at 300 °C for 2 h.

Silver impregnation

The biocompatible supports and silver nitrate precursor (Sigma Aldrich, >99%) were combined in an incipient wetness technique. Slurries of the support and $AgNO_3$ were prepared to give nominal silver loadings of 0.05–10 wt%; 5 g of each support were placed in a 250 cm^3 beaker along with the required mass of silver nitrate and stirred in 50 cm^3 deionised water at 350 rpm for 24 h. The resulting paste was oven dried at 100 °C and then left to air dry for a further 24 h. Samples were then heated in flowing air at 10 °C min^{-1} to 500 °C and calcined for 3 h. The brilliant white

[a]*Department of Chemistry, University of York, York, UK YO10 5DD*
[b]*Cardiff Catalysis Institute, School of Chemistry, Cardiff, UK CF10 3AT. E-mail: leeaf@cardiff.ac.uk; Fax: +44 (0)2920 874778; Tel: +44 (0)2920 874778*
[c]*Sincotrone Trieste, 34149 Basovizza, Trieste, Italy*

† Electronic supplementary information (ESI) available: Additional characterisation of HA materials, ZoI images and comparative microactivity tests. See DOI: 10.1039/c0jm01500h

 This journal is © The Royal Society of Chemistry 2010

parent supports appeared off-white following low Ag loadings and light sand coloured following high Ag loadings.

Physical characterisation

Elemental analysis was conducted using a Hitachi Z-5300 Polarised Zeeman AA, calibrated with silver AA standard solutions (Aldrich, 1000 μg cm^{-3} Ag in 1 wt% HNO_3). Known amounts of test sample were digested in warm, concentrated HNO_3 acid, and analysed in triplicate to improve accuracy.

Porosimetry was conducted on a Quantasorb Nova instrument by N_2 physisorption. Surface areas were calculated using the BET equation over the pressure range $P/P_0 = 0.02$–0.2, where a linear relationship was maintained, while pore-size distributions were calculated using the BJH model up to $P/P_0 = 0.95$. Samples were degassed under vacuum at 120 °C for at least 2 h prior to analysis. Powder X-ray patterns were recorded using a Bruker AXS D8 diffractometer equipped with a Cu Kα X-ray source and LynxEye™ detector. Data were collected over $2\theta = 20$–70° with a step size of 0.02°. TEM was conducted on a Philips EM 208 instrument operating at 80 kV. Samples were dispersed and sonicated in ethanol, and evaporated onto continuous carbon film grids.

Ag K-edge (25.5 keV) XANES measurements were made on the XAFS beamline of the Elettra synchrotron facility, using a Si(111) double-crystal monochromator with a beam current/energy of 250 mA per 2 GeV. Additional XAS measurements were made on Station 9.3 of the Daresbury SRS using a Si(220) double-crystal monochromator with a beam current/energy of 150 mA per 2 GeV. Transmission and fluorescence Ag K-edge spectra were acquired on powdered samples mounted within stainless steel washers. Silver standards were diluted with boron nitride to achieve unit absorbance. Linear combination fitting of the Ag-impregnated supports XANES data to Ag_2O, AgO, Ag_3PO_4, Ag_2CO_3 and Ag foil standards was undertaken with the Athena 0.8.050 application from the IFEFFIT Open Source software suite.[36] EXAFS of HA samples and silver standards were background subtracted and fitted using the Daresbury Exspline and Excurv98 packages.

Dissolution kinetics

A Nico 2000 Silver Ion-Selective Electrode (ISE) was employed for measuring dissolved Ag^+ as a function of time. The electrode was calibrated against a series of known standard solutions spanning 5, 10, 50, 100 and 1000 ppm using silver atomic absorption standard solutions (Aldrich, 1000 μg cm^{-3} Ag in 1 wt% HNO_3). Analyses were performed in a 0.1 M buffer solution of $NaNO_3$. 50 mg of Ag standard or 200 mg of Ag supported on HA were stirred in 25 cm^3 of deinionised water at room temperature. 5 cm^3 aliquots of this sample were then periodically added to 25 cm^3 of 0.1 M $NaNO_3$ solution to determine the Ag^+ concentration from the sample. Direct measurement in the sample beaker was not possible as the electrode could not tolerate powders.

Microbiological studies

Zone of Inhibition (ZoI) plates were prepared by seeding agar plates with a known number of bacteria (~10^8 colony forming units per cm^3), and known amounts of powder samples subsequently placed on the seeded agar. Tests were performed against two bacterial strains, *Staphyloccocus aureus* NCTC 10788 and *Pseudomonas aeruginosa* NCIMB 8626, examples of Gram-positive and Gram-negative bacteria common in chronic wounds. The test organisms were harvested from overnight cultures grown at 37 °C on fresh tryptone soya agar (TSA, a nutrient-rich, soyabean casein digest agar widely used to cultivate microorganisms) slopes. Test organisms were harvested into 9 ml Ringers solution (containing sodium, iron and potassium) and washed twice. The test suspensions were adjusted to give the desired bacterial inoculum of 10^8 colony forming units per cm^3 (cfu cm^{-3}). The colony density was confirmed by performing 10-fold serial dilutions of the test suspension to a 10^{-8} factor, and plating the last three dilutions *via* the pour plate method. In the pour plate method, 1 cm^3 of the required dilution is pipetted into Petri dishes and ~20 ml TSA added. Plates are then incubated at 37 °C for 24 h to allow growth of colonies which can be manually counted and the original bacterial concentration thus deduced.

Zone plates were prepared by pouring 140 ml of Mueller Hinton agar (MHA, an infusion of beef and acid hydrolysate of casein) into a 23 × 23 cm assay plate. Once set, a second 140 ml of MHA were seeded with 1.4 cm^3 of the 10^8 cfu cm^{-3} suspension of chosen test organism (final concentration ~10^6 cfu ml^{-1}) which was mixed gently and poured over the previous layer. Once this layer had set, plates were dried at 37 °C for 30 minutes with the lid removed, and then 8 mm wells bored into the agar. The bore was first dipped in 70% ethanol and heated to high temperature to minimise contamination, and 8 mm agar disks removed with a sterile micro-spatula. 200 μl of sterile water were added to each 10 mg HA sample to be tested and the slurry pipetted into wells. Assay plates were finally sealed with lab film and incubated for 24 h at 37 °C.

More quantitative Log reduction tests were also performed with *S. aureus* NCTC 10788. This was harvested by the above method to yield an inoculum of 10^7 cfu cm^{-3}. In duplicate, 10 mg of Cap/Hap sample were inoculated with 0.5 ml of this inoculum in sterile universals. These samples were incubated at 32 °C for varying intervals (24, 72 or 168 h). At each time point STS was added, to instantly passivate any dissolved silver (validation of neutralisation was checked using the ISE, in order to ensure that STS would fully inhibit any antimicrobial activity arising from soluble Ag^+). The resulting solution was serially diluted to obtain a range of countable dilutions. A baseline zero time count was always carried out immediately following inoculation as a double-check on the calculated log reduction. Following incubation, colonies were counted and multiplied up by the appropriate dilution factor to determine the original colony count remaining in the neat sample. The log count of microorganisms present at each time point can be subtracted from the log count present at zero time to yield the log reduction. One log reduction unit equates to a 90% decrease in the number of bacteria; the industry standard requirement for a material to be classified as antibacterial is three log reduction units, corresponding to a 99.9% reduction in numbers of viable bacteria, with typical household disinfectants affording >5-fold log reduction.[37]

Published on 16 August 2010 on http://pubs.rsc.org | doi:10.1039/C0JM01500H
Downloaded by Cardiff University on 02 April 2012

Published on 16 August 2010 on http://pubs.rsc.org | doi:10.1039/C0JM01500H
Downloaded by Cardiff University on 02 April 2012

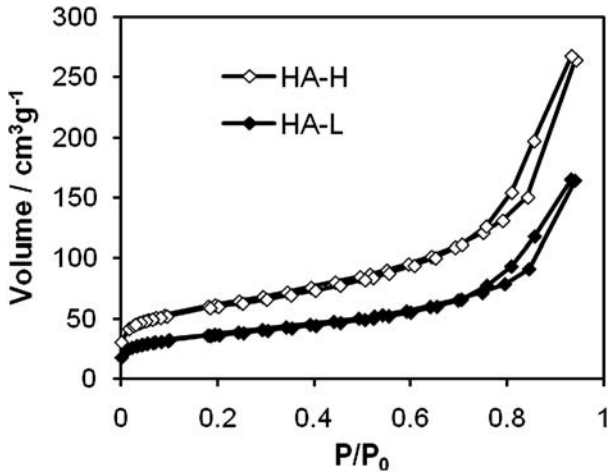

Fig. 1 Adsorption–desorption isotherms of parent HA supports.

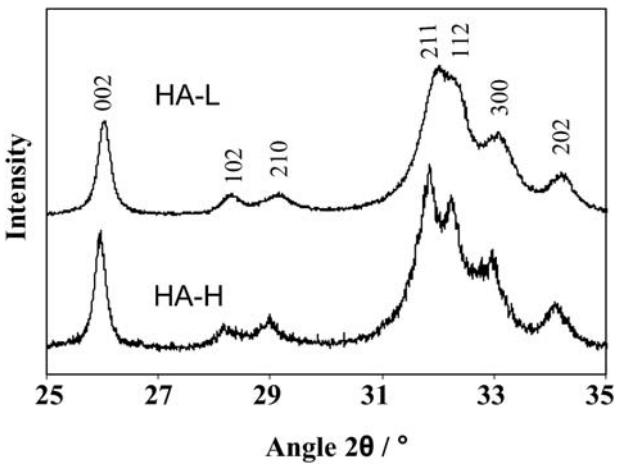

Fig. 2 Powder X-ray diffractograms of parent HA supports, indexed against JCPS 9-432.

Results and discussion

HA supports

Physico-chemical properties of both parent supports were first evaluated to confirm the successful synthesis of high and low area HA. Porosimetry revealed both supports exhibited Type IV isotherms, characteristic of micro-mesoporous solids, with hysteresis loops indicative of cylindrical pore openings (Fig. 1). The HA-L surface area was only 63 $m^2 g^{-1}$, much lower than the corresponding HA-H support, which at 204 $m^2 g^{-1}$ is significantly higher than previously reported for alternative nanocrystalline HA materials.[38–40] These differing HA surface areas are expected to strongly influence subsequent silver dispersion. Pore diameters ranged from 1–20 nm for HA-L, while HA-H exhibited a sharper pore-size distribution, centred ~6.5 nm in accordance with TEM. BJH analysis indicates around 70% of the HA-H surface area arises from mesopores.

Powder XRD showed both HA materials were crystallographically identical (Fig. 2), matching well to literature patterns for pure hydroxyapatite (JCPDS 9-432). HA-H possesses a higher degree of crystallinity, associated with larger mean particle diameters of 37 nm compared with 30 nm for HA-L (estimated from peak broadening using the Scherrer equation). The surface Ca : P atomic ratios determined by XPS were also in line with expectations at ~1.53 for both samples, slightly lower than the theoretical value of 1.67 for pure HA, but greater than that expected for α- and β-tricalcium phosphates and in line with previous reports.[41]

Structural properties of Ag-doped HA

Following the successful synthesis of HA supports of variable surface areas, HA-L and HA-H were both doped with a series of silver concentrations nominally between 0.05 and 10 wt%. The resulting bulk and surface Ag loadings are given in Table 1, from which it is evident that the similar (tuneable) silver concentrations could be achieved for both HA supports without significant silver surface segregation, indicating a uniform distribution of Ag throughout the porous matrices.

Porosimetry (ESI†) showed negligible textural changes following silver incorporation, although surface areas fell slightly with increasing Ag loading giving maximal decreases of ~10 $m^2 g^{-1}$ and 50 $m^2 g^{-1}$ for HA-L and HA-H, respectively. These decreases likely reflect micropore blockage by Ag-containing nanoparticles. Evidence for the latter was obtained from complementary XRD, XPS and XAS measurements of the

Table 1 Silver content of doped HA samples

Nominal Ag loading (wt%)	HA-L bulk[a] (wt%)	HA-H bulk[a] (wt%)	HA-L surface[b] (wt%)	HA-H surface[b] (wt%)
0.05	0.07	0.05	0.16	0.13
0.5	0.29	0.31	0.43	0.34
1	0.69	0.58	0.67	0.48
2.5	1.19	1.39	1.38	1.32
5	3.03	3.27	3.23	3.48
10	6.87	5.56	6.69	6.01

[a] Determined by atomic absorption. [b] Determined by XPS.

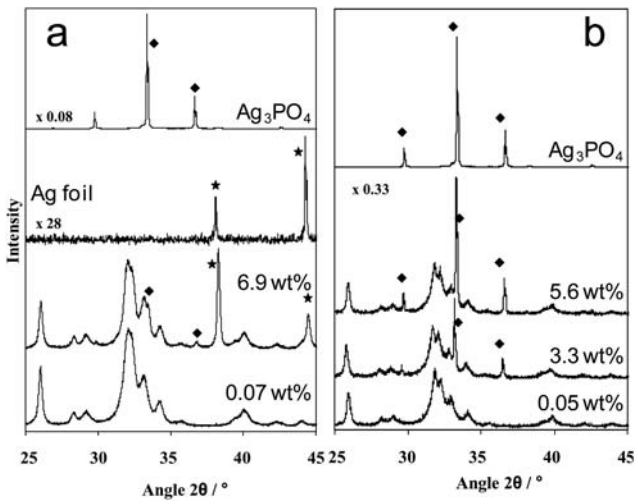

Fig. 3 Powder X-ray diffractograms of (a) Ag–HA-L and (b) Ag–HA-H and comparative bulk Ag_3PO_4 (◆) and Ag metal (★) standards.

This journal is © The Royal Society of Chemistry 2010

Published on 16 August 2010 on http://pubs.rsc.org | doi:10.1039/C0JM01500H
Downloaded by Cardiff University on 02 April 2012

Ag-doped HAs. Fig. 3a and b compare XRD patterns of representative Ag–HA samples and standards. No silver derived reflections were visible below 3 wt%, consistent with formation of highly dispersed (<3 nm) particles. TEM confirmed the presence of uniformly distributed sub-4 nm particles. For the HA-L sample, higher loadings resulted in weak XRD features associated with Ag_3PO_4 particles (45 nm mean diameter) and stronger reflections arising from metallic silver (60 nm). These coincide with the appearance of large (>10 nm) Ag crystallites by TEM. In contrast, only Ag_3PO_4 nanoparticles were observed on the HA-H support, with their intensity and size increasing with Ag content, reaching ~40 nm for the 5.56 wt% sample. There was no evidence for bulk silver oxides or carbonate. Silver phosphate nanoparticles have been previously observed over Ag-doped, microwave synthesised HA nanowhiskers,[33] and pre-formed HA porous sinters,[22] in competition with Ag^+ lattice substitution for Ca^{2+} ions. Here we note that higher surface area HA thus appears to preferentially stabilise silver phosphate nanoparticles. These observations are consistent with XPS measurements of both series, which show surface Ag_3PO_4 and Ag_2CO_3 co-exist at high silver loadings (Fig. 4), with the surface phosphate concentration increasing with silver dispersion (decreasing Ag loading). There was no evidence of surface silver metal or oxides, in contrast to literature reports for wet impregnation of conventional, low area (50 m^2 g^{-1}) HA,[42] however, good spectral fits could not be achieved without incorporating an additional high binding component at 368.5 eV that could not be matched with any feasible bulk silver standard. This new component may reflect either the genesis of a new chemical environment, *e.g.* Ag_3PO_4 localised at the support interface (initial state effects), or changes in core–hole neutralisation efficiency arising from *e.g.* particle size-effects and poorer screening of sub-10 nm Ag_3PO_4 clusters (final state effects); nanoparticle silver orthophosphate is known to possess

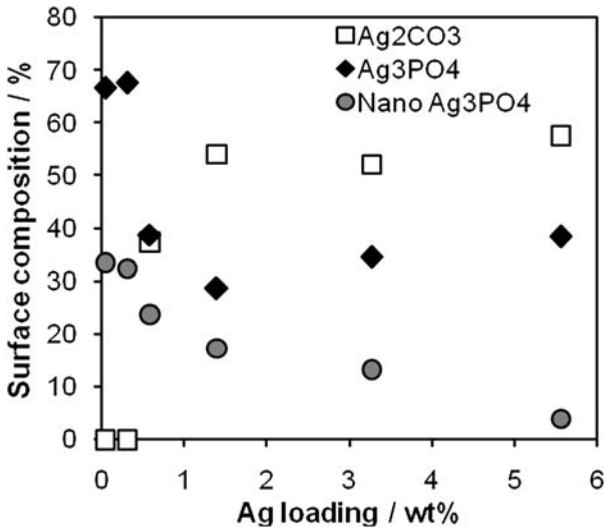

Fig. 5 Surface concentrations of silver species derived from fitted Ag 3d XP spectra of Ag–HA-H as a function of bulk silver loading.

unusual electronic properties.[43] In either case, the loading dependence of this new silver feature, quantified in Fig. 5 for Ag–HA-H, suggests it is characteristic of nanostructured silver phosphate; the corresponding C 1s spectra discount any form of perturbed surface carbonate. The choice of HA support has little influence upon the distribution of surface silver species, with a common limiting composition of 65% Ag_3PO_4/35% nano-Ag_3PO_4 attained for the highest dispersions.

XANES provided further insight into the (average) local chemical environment of Ag atoms dispersed across the HA supports. Fig. 6 presents normalised Ag K-edge XANES as a function of silver loading. High loadings favour the formation

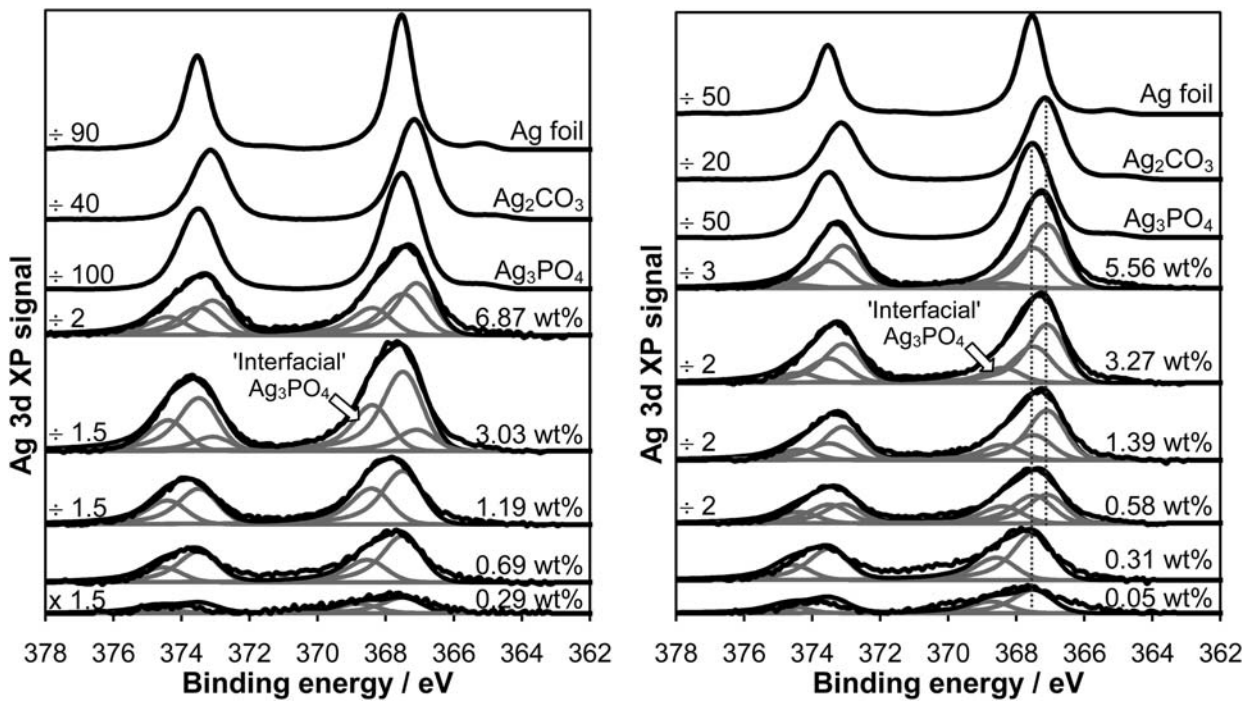

Fig. 4 Fitted Ag 3d XP spectra of (left) Ag–HA-L and (right) Ag–HA-H and comparative bulk silver standards.

Published on 16 August 2010 on http://pubs.rsc.org | doi:10.1039/C0JM01500H
Downloaded by Cardiff University on 02 April 2012

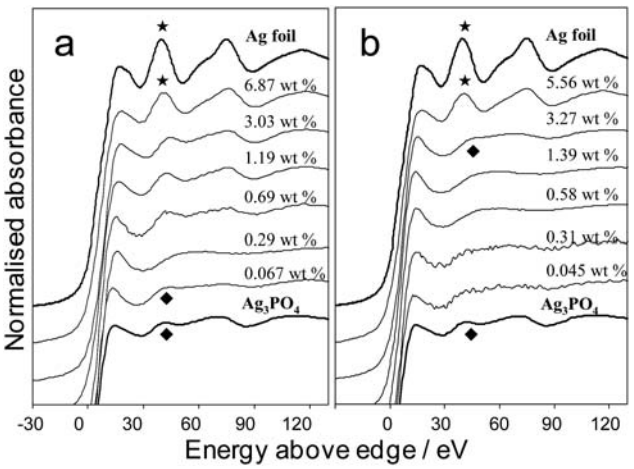

Fig. 6 Normalised Ag K-edge XANES of (a) Ag–HA-L and (b) Ag–HA-H and comparative bulk silver standards.

of metallic silver nanoparticles over HA-L, in agreement with XRD, with phosphate-like features only emerging at the lowest loadings.[44] While Ag metal is also observed for the 5.56 wt% Ag–HA-H sample, these features vanish for all lower silver loadings, which closely resemble bulk Ag_3PO_4.

These trends were quantified through linear combination fitting of each Ag–HA sample to reference compounds (ESI†). The resulting compositional analysis is shown in Fig. 7 for both supports. All spectra fitted well to simple silver metal/phosphate mixtures, with negligible contributions from either Ag_2O, AgO or $AgCO_3$. While both supports show the same qualitative behaviour, it is again evident that HA-H permits a higher absolute concentration of Ag_3PO_4 nanoparticles. Detailed EXAFS analysis (ESI†) confirmed our phase assignments, revealing an excellent fit to fcc silver metal for high Ag loadings on HA-L and a corresponding good fit to crystalline Ag_3PO_4[45] for all but the highest HA-H loading sample (representative radial distribution functions are shown in Fig. 8a and b).

Silver dissolution kinetics for Ag-doped HA

Having discovered that the choice of HA support influences both the dispersion and the nature of nanoparticulate silver phase, the question arises whether these differences influence subsequent silver dissolution (a pre-requisite to bactericidal action). Silver release rates were therefore assayed using an electrochemical ion-selective electrode by measuring the increase in [Ag^+] with time. The resulting rates in Fig. 9 were derived from the initial linear portion of the dissolution profile, and are normalised to the mass of silver in each parent sample or reference compound for quantitative comparison.

The correlation between silver loading and solubility is striking; dilute Ag–HA samples release ionic silver orders of magnitude faster than their high loading counterparts *independently of the support*. This trend tracks the associated (surface and bulk) Ag_3PO_4 content, with the HA-H materials, which for any given Ag loadings contain proportionally more phosphate, releasing Ag^+ fastest. Dissolution profiles were also obtained for related silver standards, including silver sulfadiazine (SSD),

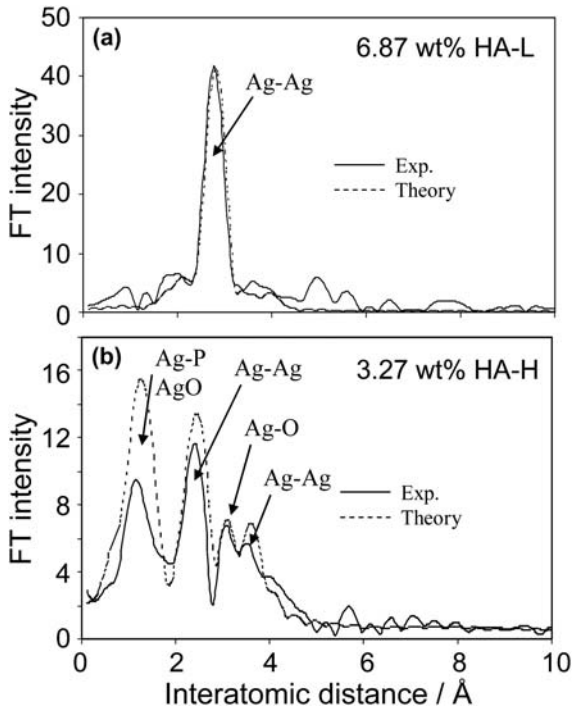

Fig. 8 Fitted Ag K-edge radial distribution functions for representative Ag–HA samples.

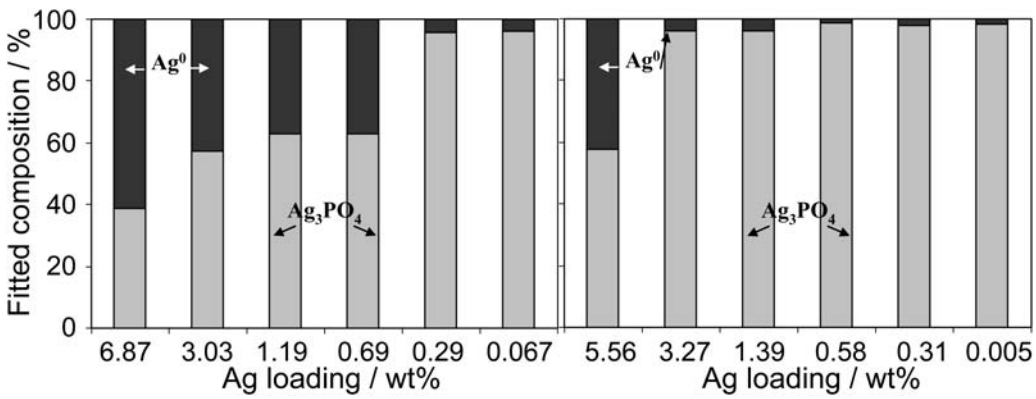

Fig. 7 Average composition of (left) Ag–HA-L and (right) Ag–HA-H derived from fitted Ag K-edge XANES.

 This journal is © The Royal Society of Chemistry 2010

Published on 16 August 2010 on http://pubs.rsc.org | doi:10.1039/C0JM01500H
Downloaded by Cardiff University on 02 April 2012

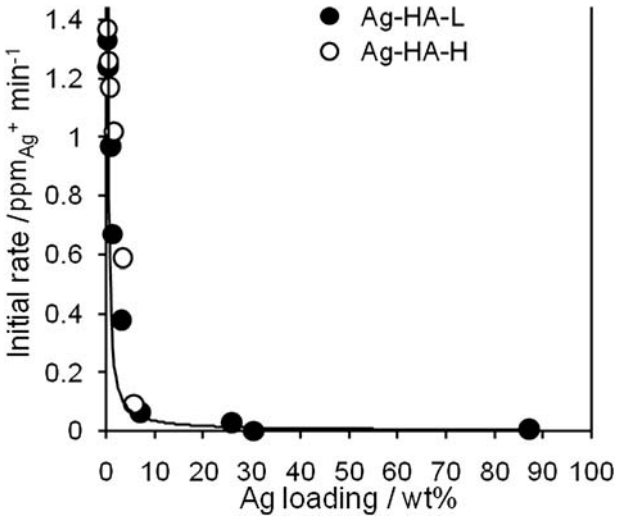

Fig. 9 Normalised initial rate of Ag^+ dissolution as a function of bulk silver loading for Ag–HA samples and reference standards.

which proved largely insoluble in the identical aqueous medium. The poor performance of pure Ag_3PO_4 reflects particle size effects (mean XRD crystallite diameter ~120 nm), which result in a very low surface area : volume ratio and thus extremely slow dissolution. SSD is likewise sparingly soluble under our conditions; its efficacy is a strong function of wound pH and the presence of sodium salts and proteins in tissue fluid. These dissolution rates also compare favourably with those from mesoporous-Al_2O_3 supported Ag_2CO_3 nanoparticles[25] wherein a maximum solubility of 1.48 ppm$_{Ag^+}$ min^{-1} was observed, and vastly exceed those observed for *e.g.* phosphate-based glasses (typically 0.2 ppm h^{-1}),[23,46] or polymer coatings.[47]

Antibacterial performance

The antimicrobial activities of the Ag–HA materials were assessed by zone plate inhibition (ZoI) and the logarithmic reduction method against *S. aureus* NCTC 10788 and *P. aeruginosa* NCIMB 8626. These represent respective Gram-positive and -negative bacteria commonly found on the skin and in chronic wounds.

In the zone assay method, antimicrobial efficacy is proportional to the size of the colony-free zone surrounding the test sample, where bacterial growth was inhibited. The results in Fig. 10a and b show a strong (inverse) correlation between silver (loading) phosphate composition and bactericidal activity for both Ag–HA materials, with almost a 100-fold enhancement achievable across each series. The higher area Ag–HA-H materials outperformed their Ag–HA-L counterparts (although ZoI tests are only semi-quantitative) against both bacterial strains, with the more resilient Gram-positive *S. aureus* proving harder to inhibit. Comparative measurements for reference bulk compounds (AgO = 0.19 mm g_{Ag}^{-1}, Ag_2O = 0.08 mm g_{Ag}^{-1} and Ag_2CO_3 = 0.1 mm g_{Ag}^{-1}) highlight the outstanding performance, per mass of silver, of our HA-supported Ag_3PO_4 nanoparticles. The plots in Fig. 10 exhibit two distinct loading regimes, mirroring the dissolution rates in Fig. 9. We associate the first region, between 5 and 1 wt% Ag, with the phase transition from

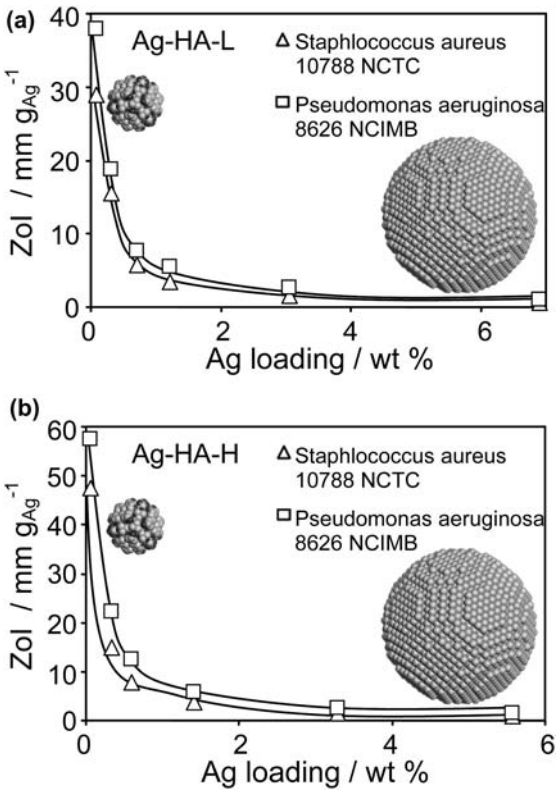

Fig. 10 Normalised zones of inhibition as a function of bulk Ag loading for Ag–HA samples.

metallic silver or phosphate bulk-like structures to nanoparticulate (<3 nm) Ag_3PO_4, and attribute the second, more pronounced region between 1 and 0.05 wt% Ag, to decreasing Ag_3PO_4 particle size and a corresponding rise in surface area and thus enhanced solubility. By way of comparison, our best performing Ag_2CO_3/meso-Al_2O_3 material gave diffusion zones of 36 mm g_{Ag}^{-1} (*S. aureus*) and 24 mm g_{Ag}^{-1} (*P. aeruginosa*),[25] both significantly lower than that observed for the lowest loading Ag–HA-H sample in Fig 9.

Although ZoI measurements are a good indicator of antimicrobial activity, they do not provide quantitative bacterial kill rates, which are far more important in *e.g.* wound management: clear zones evidence bacterial inhibition but not necessarily cytotoxicity. Quantitative log reduction kill tests were therefore subsequently undertaken to assess the potency of Ag–HA samples against *S. aureus* over 7 days. In this approach, a known concentration of microorganisms (10^7 cfu ml^{-1}) was added to the test material, and then recovered after different time periods and cultured. Antimicrobial activity is assayed from the decrease in viable bacteria after specific times: each increasing $\log_{10}$ reduction unit equates to a 90% enhanced kill rate over the preceding value. The resulting time dependent log reductions are shown in Fig. 11 for both HA series, alongside a range of pure silver compounds. The first important observation is that all the dispersed Ag–HA materials significantly outperform any of the unsupported silver compounds. Of these latter controls, pure Ag_2CO_3 and Ag_3PO_4 exhibited the highest antibacterial activity, but still lagged at least 0.5 log reduction units behind the worst performing 6.87 wt% Ag–HA-L sample. Second, *activity*

systematically increases with decreasing silver content over both HA supports, in line with the silver release rates and ZoI results; these trends were also maintained across the entire 7-day test period. This finding is in accordance with our observations of Ag-doped aluminas, wherein the lower the silver concentration the higher the bactericidal efficacy. Our prediction that 'less precious metal = improved antibacterial performance' (per unit mass of Ag) may have cost/benefit implications for formulating new Ag-containing medical devices, particularly silver-based wound dressings,[48] wherein existing commercial products offer a wide range of loadings spanning 1.6–546 mg Ag per100 cm^2.[49] It is worth noting that despite the excellent water solubility of $AgNO_3$ (ESI†), consequent high [Ag+] can drive colloidal silver formation (often as a 'silver mirror'), hence the exceptional performance of our Ag–HA materials cannot be accounted for by their fast release of Ag(I) ions alone. Some studies have postulated that colloidal silver may interact directly with pathogens to promote cell death.[50] However, there remains little evidence for a specific Ag-bacterial interaction, *e.g.* localised accumulation of silver within cell walls or unique intracellular compartments, with uniform bacterial decoration by silver nanoparticles more indicative of non-specific electrostatic interactions. Since we observe an inverse correlation between the formation of metallic silver and bactericidal activity, it seems more plausible that phosphate ions (released alongside ionic silver) contribute to additional disruption of cellular metabolic pathways. Fig. 11 also highlights that each Ag–HA-H sample outperformed its analogous loading Ag–HA-L counterpart by >0.5 log reduction units following the 7-day test, which we attribute to a higher proportion of more highly dispersed ionic Ag(I) species. This conclusion is supported by the relative antibacterial potencies of our previous alumina-supported silver

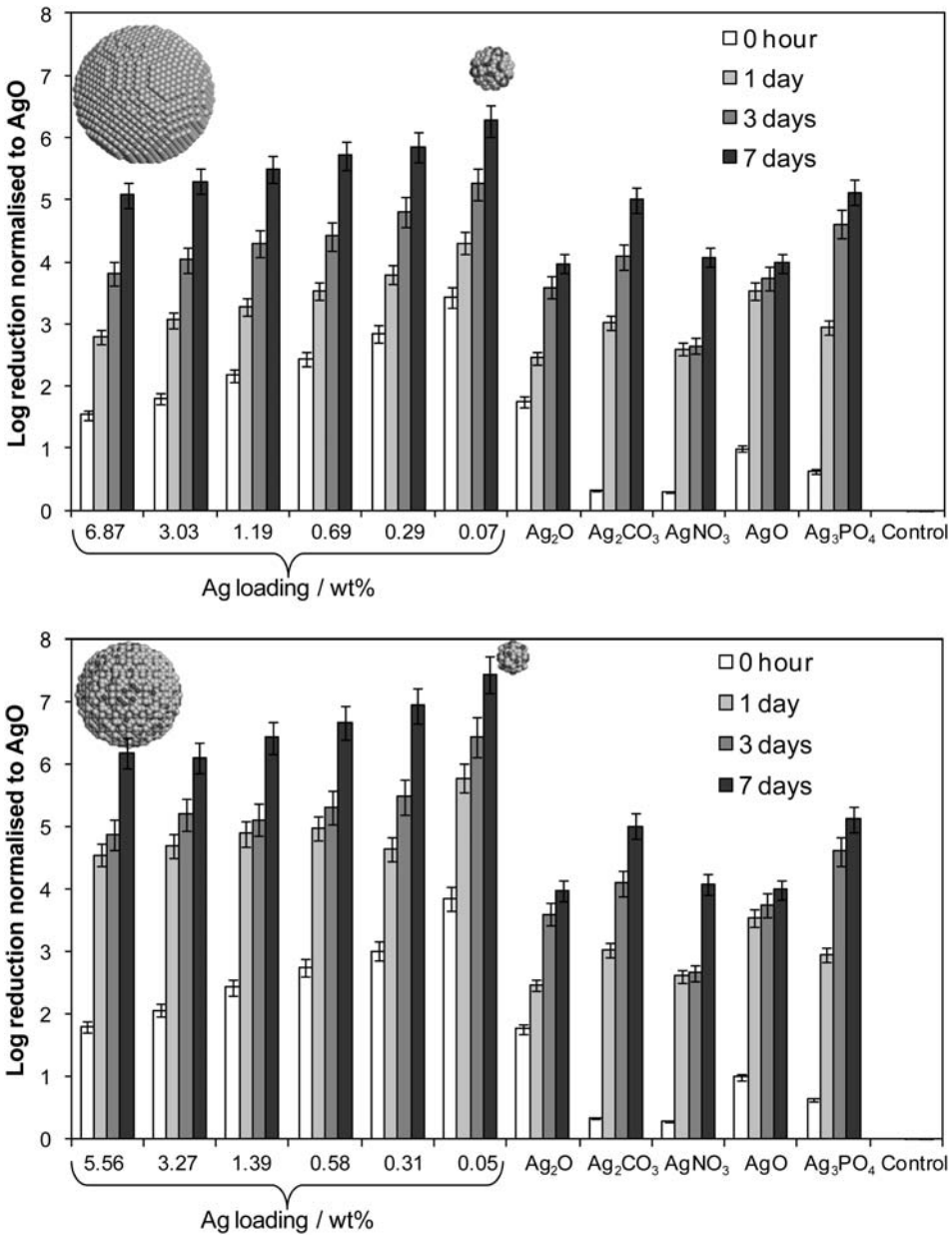

Fig. 11 Normalised zones of inhibition as a function of bulk Ag loading for Ag–HA–L (top) and Ag–HA–H (bottom) samples and reference standards.

Published on 16 August 2010 on http://pubs.rsc.org | doi:10.1039/C0JM01500H
Downloaded by Cardiff University on 02 April 2012

 This journal is © The Royal Society of Chemistry 2010

Published on 16 August 2010 on http://pubs.rsc.org | doi:10.1039/C0JM01500H
Downloaded by Cardiff University on 02 April 2012

materials,[25] for which the hierarchy follows: Ag–HA-H > Ag–mesoporous-Al_2O_3 > Ag–HA-L > Ag-γ-Al_2O_3 (ESI†). High surface area supports (HA-H or meso-alumina = 204 or 350 m^2 g^{-1} respectively) thus appear to promote stabilisation of Ag(I) nanocrystallites with respect to conventionally synthesised low area supports (HA-L or γ-alumina = 204 or 180 m^2 g^{-1} respectively). The better performance of nanoparticulate Ag_3PO_4 (stabilised on HA) *versus* nanoparticulate Ag_2CO_3 (stabilised on alumina) is still not understood, and likely reflects a combination of factors including support hydrophilicity/surface charge, and influence of dissolved carbonate and phosphate counter ions on solution pH and Ag^+ solubility. We are currently developing methods to incorporate our Ag–HA powders into more easily processed presentation formats for clinical tests.

Conclusions

Silver impregnation of porous hydroxyapatites provides a simple means to control the production of dispersed Ag(I) species for antibacterial applications. The use of low surface area HA, or high Ag loadings, generates inhomogeneous materials containing large (>45 nm) metallic and/or phosphate particles which exhibit slow dissolution kinetics and poor microbiological performance against Gram-negative and -positive bacteria. High area HA, or ultra-dilute silver loadings (<0.5 wt% Ag), preferentially stabilise sub-3 nm pure Ag_3PO_4 nanoparticles with dramatically enhanced silver release rates and corresponding bacterial kill rates.

Acknowledgements

We thank the Engineering and Physical Sciences Research Council (EP/G007594/2), Sincrotrone Trieste (beamtime award 2006685) and Daresbury SRS for financial support. A.F.L. thanks the EPSRC for the award of a Leadership Fellowship and J.J.B. thanks Smith & Nephew for studentship support. We also express our gratitude to Dr Ian Harvey (previously of Daresbury SRS) for assistance with XAS measurements and Dr Bryan Greener (Smith & Nephew) for valuable discussions and support of our research programme.

Notes and references

1 M. Jarcho, *Clin. Orthop. Relat. Res.*, 1981, (157), 259–278.
2 D. W. Hutmacher, *Biomaterials*, 2000, **21**, 2529–2543.
3 Q. Peng, F. X. Jiang, P. Huang, S. B. Zhou, J. Weng, C. Y. Bao, C. Zhang and H. Y. Yu, *J. Biomed. Mater. Res., Part A*, 2010, **93**, 920–929.
4 P. S. Stewart, *Lancet*, 2003, **361**, 97.
5 P. S. Stewart and J. W. Costerton, *Lancet*, 2001, **358**, 135–138.
6 N. Cerca, S. Martins, G. B. Pier, R. Oliveira and J. Azeredo, *Res. Microbiol.*, 2005, **156**, 650–655.
7 D. Mack, H. Rohde, L. G. Harris, A. P. Davies, M. A. Horstkotte and J. K. M. Knobloch, *Int. J. Artif. Organs*, 2006, **29**, 343–359.
8 Z. H. Chohan, M. Arif, M. A. Akhtar and C. T. Supuran, *Bioinorg. Chem. Appl.*, 2006, 83131.
9 N. Jones, B. Ray, K. T. Ranjit and A. C. Manna, *FEMS Microbiol. Lett.*, 2008, **279**, 71–76.
10 J. Duffy, *The Sanitarians: a History of American Public Health*, University of Illinois Press, 1992.
11 C. A. Moyer, L. Brentano, D. L. Gravens, H. W. Margraf and W. W. Monafo, *Arch. Surg. (Chicago, IL, U. S.)*, 1965, **90**, 812–867.
12 C. L. Fox, B. W. Rappole and W. Stanford, *Surg., Gynecol. Obstet.*, 1969, **128**, 1021–1026.
13 H. S. Carr, T. J. Wlodkows and H. S. Rosenkra, *Antimicrob. Agents Chemother.*, 1973, **4**, 585–587.
14 K. Kawahara, K. Tsuruda, M. Morishita and M. Uchida, *Dent. Mater.*, 2000, **16**, 452–455.
15 C. Hansel, G. Leyhausen, U. E. M. Mai and W. Geurtsen, *J. Dent. Res.*, 1998, **77**, 60–67.
16 J. J. Blaker, S. N. Nazhat and A. R. Boccaccini, *Biomaterials*, 2004, **25**, 1319–1329.
17 C. L. Fox and S. M. Modak, *Antimicrob. Agents Chemother.*, 1974, **5**, 582–588.
18 Q. L. Feng, J. Wu, G. Q. Chen, F. Z. Cui, T. N. Kim and J. O. Kim, *J. Biomed. Mater. Res.*, 2000, **52**, 662–668.
19 F. Furno, K. S. Morley, B. Wong, B. L. Sharp, P. L. Arnold, S. M. Howdle, R. Bayston, P. D. Brown, P. D. Winship and H. J. Reid, *J. Antimicrob. Chemother.*, 2004, **54**, 1019–1024.
20 S. Tarimala, N. Kothari, N. Abidi, E. Hequet, J. Fralick and L. L. Dai, *J. Appl. Polym. Sci.*, 2006, **101**, 2938–2943.
21 S. D. Oh, S. Lee, S. H. Choi, I. S. Lee, Y. M. Lee, J. H. Chun and H. J. Park, *Colloids Surf., A*, 2006, **275**, 228–233.
22 L. Yang, X. S. Ning, Q. F. Xiao, K. X. Chen and H. P. Zhou, *J. Biomed. Mater. Res., Part B*, 2007, **81**, 50–56.
23 S. P. Valappil, J. C. Knowles and M. Wilson, *Appl. Environ. Microbiol.*, 2008, **74**, 5228–5230.
24 A. B. G. Lansdown, *Brit. J. Nurs.*, 2004, **13**, S6.
25 J. J. Buckley, P. L. Gai, A. F. Lee, L. Olivi and K. Wilson, *Chem. Commun.*, 2008, 4013–4015.
26 S. L. Percival, P. Bowler and E. J. Woods, *Wound Repair Regen.*, 2008, **16**, 52–57.
27 J.-Y. Maillard and S. P. Denyer, *European Wound Management Association Journal*, 2006, **6**, 5–9.
28 J. K. Liu, X. H. Yang and X. G. Tian, *Powder Technol.*, 2008, **184**, 21–24.
29 M. Diaz, F. Barba, M. Miranda, F. Guitian, R. Torrecillas and J. S. Moya, *J. Nanomater.*, 2009, 498505.
30 Y. Ando, H. Miyamoto, I. Noda, N. Sakurai, T. Akiyama, Y. Yonekura, T. Shimazaki, M. Miyazaki, M. Mawatari and T. Hotokebuchi, *Mater. Sci. Eng., C*, 2010, **30**, 175–180.
31 M. Shirkhanzadeh, M. Azadegan and G. Q. Liu, *Mater. Lett.*, 1995, **24**, 7–12.
32 R. J. Chung, M. F. Hsieh, K. C. Huang, L. H. Perng, F. I. Chou and T. S. Chin, *J. Sol-Gel Sci. Technol.*, 2005, **33**, 229–239.
33 N. Rameshbabu, T. S. S. Kumar, T. G. Prabhakar, V. S. Sastry, K. Murty and K. P. Rao, *J. Biomed. Mater. Res., Part A*, 2007, **80**, 581–591.
34 A. Bahadir, C. Ergun and M. Baydogan, in *Diffusion in Solids and Liquids IV*, ed. A. Ochsner, G. E. Murch and A. Shokuhfar, Trans Tech Publications, Switzerland, 2009, pp. 250–255.
35 L. El Hammari, H. Merroun, T. Coradin, S. Cassaignon, A. Laghzizil and A. Saoiabia, *Mater. Chem. Phys.*, 2007, **104**, 448–453.
36 B. Ravel and M. Newville, *J. Synchrotron Radiat.*, 2005, **12**, 537–541.
37 F. B. Sally, M. Arthur, K. Begun and H. Patel, *Lett. Appl. Microbiol.*, 1993, **17**, 119–125.
38 S. Bose and S. K. Saha, *Chem. Mater.*, 2003, **15**, 4464–4469.
39 C. Hoffmann, C. Zollfrank and G. Ziegler, *J. Mater. Sci.: Mater. Med.*, 2008, **19**, 907–915.
40 H. C. Shum, A. Bandyopadhyay, S. Bose and D. A. Weitz, *Chem. Mater.*, 2009, **21**, 5548–5555.
41 H. B. Lu, C. T. Campbell, D. J. Graham and B. D. Ratner, *Anal. Chem.*, 2000, **72**, 2886–2894.
42 P. A. Kumar, M. P. Reddy, L. K. Ju and H. H. Phil, *Catal. Lett.*, 2008, **126**, 78–83.
43 M. Thomas, S. K. Ghosh and K. C. George, *Mater. Lett.*, 2002, **56**, 386–392.
44 I. Ahmed, E. A. Abou Neel, S. P. Valappil, S. N. Nazhat, D. M. Pickup, D. Carta, D. L. Carroll, R. J. Newport, M. E. Smith and J. C. Knowles, *J. Mater. Sci.*, 2007, **42**, 9827–9835.
45 M. N. Deschizeauxcheruy, J. J. Aubert, J. C. Joubert, J. J. Capponi and H. Vincent, *Solid State Ionics*, 1982, **7**, 171–176.
46 S. P. Valappil, D. M. Pickup, D. L. Carroll, C. K. Hope, J. Pratten, R. J. Newport, M. E. Smith, M. Wilson and J. C. Knowles, *Antimicrob. Agents Chemother.*, 2007, **51**, 4453–4461.
47 J. Wang, H. X. Li, L. Ren, A. S. Zhao, P. Li, Y. X. Leng, H. Sun and N. Huang, *Surf. Coat. Technol.*, 2007, **201**, 6893–6896.
48 J. L. David, *Int. Wound J.*, 2006, **3**, 282–294.
49 S. Thomas and P. McCubbin, *J. Wound Care*, 2003, **12**, 305–308.
50 I. Sondi and B. Salopek-Sondi, *J. Colloid Interface Sci.*, 2004, **275**, 177–182.